Earth and Planetary Science Letters 302 (2011) 227–235

Contents lists available at ScienceDirect

Earth and Planetary Science Letters

journal homepage: www.elsevier.com/locate/epsl

Thermal annealing mechanisms of latent fission tracks: Apatite *vs.* zircon

Weixing Li [a,b,c], Lumin Wang [a,b], Maik Lang [c], Christina Trautmann [d], Rodney C. Ewing [a,b,c,*]

[a] Department of Materials Science and Engineering, University of Michigan, Ann Arbor, MI 48109-2104, USA
[b] Department of Nuclear Engineering and Radiological Sciences, University of Michigan, Ann Arbor, MI 48109-2104, USA
[c] Department of Geological Sciences, University of Michigan, Ann Arbor, MI 48109-1005, USA
[d] GSI Helmholtz Centre for Heavy Ion Research, Planckstr.1, 64291 Darmstadt, Germany

ARTICLE INFO

Article history:
Received 13 September 2010
Received in revised form 5 December 2010
Accepted 6 December 2010
Available online 3 January 2011

Editor: T.M. Harrison

Keywords:
in situ thermal annealing
Rayleigh instability
Brownian motion
crystallographic effect
apatite
zircon

ABSTRACT

Fission tracks in apatite and zircon, the minerals most often used for fission track dating and thermochronology, have been considered to anneal by the same mechanism, essentially epitaxial recrystallization. In this study, direct, atomic-scale observations of thermal annealing of unetched, latent tracks at elevated temperatures by transmission electron microscopy (TEM) demonstrate that the annealing behavior of tracks in apatite is entirely different from that of the amorphous tracks in zircon. Remnants of the latent tracks in apatite can be seen after *in situ* heating at 700 °C for 130 min, in clear contrast to the complete disappearance of tracks after they have been annealed at 360 °C for 1 h and then enlarged by chemical etching. The "fading" or shrinkage of tracks in apatite results from thermo-emission of vacancies from the porous core to the surrounding matrix, in contrast to the recombination of interstitials and vacancies within the amorphous tracks in zircon. The high surface energy and high diffusivity of atoms at the surface of the essentially porous tracks in apatite cause the discontinuity in the tracks by several different mechanisms: Rayleigh instability, Brownian motion, and preferential motion of track segments. The preferential motion of atoms along the *c*-axis accounts for more rapid annealing of fission tracks perpendicular to the *c*-axis of apatite. In addition to the shrinkage, the discontinuity of fission tracks in apatite prevents solutions from entering into the porous tracks for further etching, thus reducing the etched track length. This accounts for the complete disappearance of etchable tracks in apatite at much lower temperatures, as compared to that of the latent tracks observed by TEM. In contrast, the amorphous tracks in zircon do not segment due to the low surface energy and low diffusivity of atoms at the track-matrix boundary. This explains the similarity between the complete disappearance of latent tracks in zircon at 830 °C after 90 min and that of etchable tracks at 800 °C after 1 h. The very different behavior of fission tracks in zircon and apatite is a direct result of differences in the internal structure of the track — the amorphous domain in zircon *vs.* the low atomic density void in apatite.

1. Introduction

Fission tracks caused by the spontaneous fission of ^{238}U in apatite and zircon, as revealed by chemical etching, are extensively used to determine the thermal history of Earth's crust (Crowley et al., 1991; Gleadow et al., 1986; Green et al., 1986; Tagami and O'Sullivan, 2005; Yamada et al., 1995). The total kinetic energy for a fission fragment pair is around 170 MeV (Fleischer, 2004), corresponding to a range of ~20 μm in fluorapatite, and of ~16 μm in zircon (SRIM, 2006). By chemical etching, the 5–10 nm wide fission tracks are enlarged to several μm, which can be directly observed by optical microscopy (Fig. 1) (Gleadow et al., 1986). During the track formation, a fission track becomes discontinuous at each end of the track trajectory, impeding chemicals for further etching (Meftah et al., 1993; Villa et al., 1999). This results in the etched lengths, ~16 μm in apatite (Green et al., 1986), ~11 μm in zircon (Yamada et al., 1995), of fresh (or unannealed) tracks being slightly shorter than the ranges calculated by SRIM. Fission tracks are used in thermochronology because the track lengths gradually shorten due to the thermal annealing at elevated temperatures below approximately 150 °C over geological time. In the laboratory, higher temperatures, e.g., 40–360 °C for apatite (Crowley et al., 1991; Green et al., 1986) and 440–800 °C for zircon (Yamada et al., 1995), are used to expedite the thermal annealing process.

The present understanding of the annealing process is largely limited to mathematical fits to data for etched track-lengths as a function of temperature, time and composition (Carlson, 1990; Crowley et al., 1991; Gleadow et al., 2002; Green et al., 1986; Laslett et al., 1987; Yamada et al., 1995). The internal structure of latent fission tracks controls the "fading" process and correspondingly the shortening of track lengths. However, the empirical equations do not reflect the relation between the internal structure of tracks and their

* Corresponding author. Department of Geological Sciences, University of Michigan, Ann Arbor, MI 48109-1005, USA. Tel.: +1 734 763 9295; fax: +1 734 647 5706.
E-mail address: rodewing@umich.edu (R.C. Ewing).

0012-821X/$ – see front matter © 2010 Elsevier B.V. All rights reserved.
doi:10.1016/j.epsl.2010.12.016

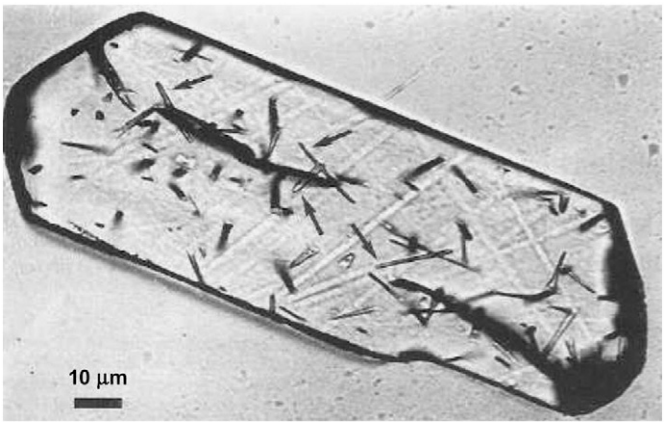

Fig. 1. An optical microscopy image of etched spontaneous tracks on a polished internal surface of apatite crystal. Arrows point to four individual confined tracks exhibiting original entire track lengths, which are useful for estimating the true length distribution (Gleadow et al., 1986).

annealing behavior because the structural information of tracks is lost due to chemical etching (Carlson, 1990; Crowley et al., 1991). Even a highly cited physical model of the process has met with considerable criticism in the absence of actual observations of the atomic-scale process (Carlson, 1990; Crowley, 1993; Green et al., 1993). Atomic-scale studies of fission track fading have long been recognized as needed for the development of quantitative models of fission track formation and annealing (Carlson, 1990; Gleadow et al., 2002; Jonckheere and Chadderton, 2002; Rabone et al., 2008).

In contrast to etched tracks, latent tracks can be directly observed by TEM, (Jaskierowicz et al., 2004), but there has been only a very limited effort to investigate the annealing behavior of latent tracks by TEM (Paul, 1993b; Paul and Fitzgerald, 1992; Price and Walker, 1962a). In the absence of atomic-scale studies, the fission tracks in apatite have been considered to be amorphous (Miro et al., 2005; Rabone et al., 2008; Tagami and O'Sullivan, 2005; Villa et al., 1999) as in other minerals, such as zircon (Lang et al., 2008). There has been no attention given to the influence of the internal structure of a track on annealing behavior. Previous efforts to compare the change in shape of single tracks after thermal treatment using the TEM were unsuccessful (Paul, 1993a). By using advanced TEM techniques, we have recently shown that the fission tracks in apatite are actually porous channels of very low atomic density instead of having the assumed amorphous core (Li et al., 2010). The formation of the "porous" core results from the irreversible decomposition of fluor-apatite, and the sublimation of volatile elements along the fission track during the highly ionizing energy deposition (Li et al., 2010; Saleh and Eyal, 2005). In this paper, the same latent tracks have been observed and studied under TEM by both *ex situ* furnace annealing and *in situ* thermal annealing over a range of temperatures. We compare the annealing behavior and mechanism of the porous tracks in apatite to that of the amorphous tracks in zircon.

2. Materials and method

Two types of tracks in fluorapatite from Durango, Mexico were investigated in this study: thermal-neutron induced fission tracks, and parallel tracks produced by exposing 50 μm thick single crystals to 2.2 GeV Au ions in 5×10^{10} ions/cm^2. TEM observations of unecthed tracks are conventionally viewed only when very high track density (up to 3×10^{10} tracks/cm^2) are present (Fleischer et al., 1975; Price and Walker, 1962b). However, the density of naturally occurring tracks created by spontaneous fission of ^{238}U in Durango apatite is too low for feasible TEM observations. A greater track density (~10^9 tracks/cm^2) was introduced into the crystal structure by thermal neutron-induced fission of ^{235}U (~10^{17} n/cm^2) in the Georgia Institute of Technology nuclear reactor. There are no fundamental differences in the nature of the tracks created by the spontaneous fission of ^{238}U or the neutron-induced fission of ^{235}U. Heavy ion irradiations were performed at the UNILAC accelerator of the GSI Helmholtz Centre for Heavy Ion Research (Darmstadt, Germany) under beam incidence parallel to the *c*-axis of the crystals. 2.2 GeV Au ions create tracks of 90 μm length much longer as compared with typical fission fragments (e.g., 100 MeV Xe ions, ~10 μm). The electronic energy loss per unit path length of ions, d*E*/d*x*, is determined by the mass and kinetic energy of the projectiles being 16 keV/nm for 100 MeV Xe ions and 26 keV/nm for 2.2 GeV Au ions. However, this difference in energy loss per unit of depth does not result in significant differences in the track morphology (Meftah et al., 1993). Parallel tracks were also produced in natural zircon from Beaune–sur-Arzon, France by exposing the single crystals to 2.2 GeV Au ions in 5×10^{10} ions/cm^2. TEM studies were conducted with a JEOL 3011 and a JEOL JEM 2010 F electron microscope. To avoid possible further irradiation-induced damage during sample thinning by ion milling, all TEM samples were crushed and suspended on a carbon film supported by Cu grid. During TEM observation, the electron current density was kept as low as possible (0.1 to 1 A/cm^2) to minimize electron–irradiation-induced microstructural changes. The high resolution TEM (HRTEM) images clearly show that the latent tracks in apatite are actually porous, significantly different from the amorphous tracks in zircon (Fig. 2). The bright core and dark fringes can be seen around a track in apatite when the TEM is at under focus condition, in which a weak lens focuses the beams slightly below the image plane (Fig. 2a). The contrast of the porous track can change into a dark core with bright fringes at the over focus condition, in which a strong lens focuses the beams slightly above the image plane (Li et al., 2010; William and Carter, 1996). The Fresnel contrast (the contrast change at different focus conditions), results from the "density jump" between the tracks and the surrounding crystalline matrix as a result of the decomposition and mass loss during the formation of the "porous" tracks (Li et al., 2010; Saleh and Eyal, 2005; William and Carter, 1996). However, the density change in the amorphous track is insignificant as compared to that of the porous track. This results in no fringes around a track in zircon (Fig. 2b), and the contrast of the track remains dark when the focus is changed. The porous track structure in apatite provides strong support for the model of "enhanced trapping" (Shuster et al., 2006) that radiogenic ^{4}He is trapped within zones of radiation damage, particularly fission tracks. It suggests that zircon, as a result of amorphous nature of fission tracks, is unlikely to show the same effect (or at least not by the same mechanism) as does apatite.

A muffle furnace was used to perform the *ex situ* thermal annealing of the fission tracks with a crushed sample sealed in an Ar-filled tube. *In situ* thermal annealing experiments were performed in the JEOL 2010 TEM equipped with a Gatan double-tilt hot-stage specimen holder with temperatures up to 1000 °C. This enabled us to directly observe high temperature fission track annealing behavior during the TEM analysis.

3. Results

3.1. The same fission tracks after ex situ annealing

Paul has reported that latent fission tracks in apatite can still be seen under TEM after heating at 450 °C for 5 h (Paul, 1993b). This is seemingly inconsistent with the optical observations that the etchable tracks completely disappeared at 360 °C for 1 h (Green et al., 1986). Thus, the observations of annealing behavior of latent tracks by TEM were thought not to correlate to those of etchable tracks observed by optical microscopy (Paul, 1993b). Resolution of this inconsistency requires that the same tracks be observed before and after the annealing experiments.

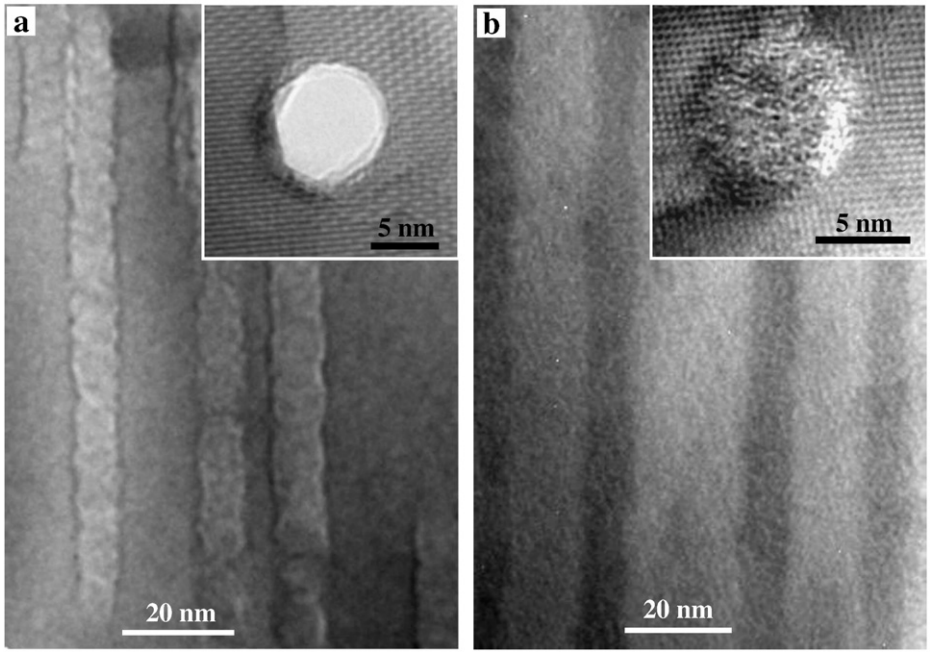

Fig. 2. TEM images of latent tracks in apatite and zircon after exposure to 2.2 GeV Au ions in 5×10^{10} ions/cm^2. (a) HRTEM image (inset) shows a porous track in apatite seen from above. The dark fringes and bright core can be seen around the parallel tracks in apatite at under focus condition. (b) The amorphous feature (inset) is obvious in the core region of tracks in zircon seen from above. No fringes can be seen around the dark core of the parallel tracks in zircon.

The same unetched fission tracks after furnace heating were observed by using a technique as shown in Fig. 3. The TEM images of fission tracks in fluorapatite were first taken from the crushed samples deposited on carbon thin film on a copper grid (Fig. 3a and b). The copper grid was then removed from the TEM and sealed in a glass tube filled with 1 atm Ar and then heated in a furnace. The grid was inserted into TEM again to find the same fission tracks after the thermal treatment. Markers were made on the copper grid in order to locate the same tracks. Two different locations are shown to reveal possible changes in morphologies of the same fission tracks before and after heating (Fig. 3c–f). However, after heating at 400 °C for 2 h, the tracks showed no obvious fading based on the comparison of the morphologies of the same tracks before and after heating. This is again seemingly inconsistent with previous optical microscopy observations of etchable track lengths in apatite, which appear to entirely disappear after heating at 360 °C for 1 h (Green et al., 1986). However, some newly formed gaps due to track fragmentation were observed as marked by the arrows (Fig. 3c–f), which may explain the lack of etchability. One can also notice the change in the relative position or relative distance between tracks, which results from the tilting of the samples deposited on the carbon film after the heating.

The annealing temperature was increased to 700 °C and maintained for 2 h in another *ex situ* thermal annealing experiment in an effort to induce a more obvious change in track morphologies. The TEM images of fission tracks before and after the heating are shown at two different locations (Fig. 4a–c). An obvious shrinkage of fission tracks in apatite can be observed (Fig. 4a and b). In addition, the fission tracks fragment into droplets, but without much periodicity (Fig. 4a and b). In another location, an obvious segmentation with periodic spacing occurs after the heating (Fig. 4c and d). The segmentation of a highly porous fission track into periodic droplets is controlled by Rayleigh instability (Glaeser, 2001; Li et al., 2010; Nichols and Mullins, 1965). Rayleigh instability is known as a harmonic perturbation of a cylindrical void in a solid or a cylindrical solid, resulting in disintegration into a row of spherical droplets spaced at ~8.89R in an idealized situation via surface diffusion (Glaeser, 2001; Nichols and Mullins, 1965). For a cylinder of radius R subjected to periodic longitudinal perturbation of wavelength λ, the amplitude α(of initially infinitesimal α_0) at time t can be given by a growth/decay law (Glaeser, 2001),

$$\alpha = \alpha_0 \exp[\mu t]. \tag{1}$$

The amplification factor

$$\mu = \frac{\delta_s D_s \gamma_s \Omega}{R^4 kT}\left[\left(\frac{2\pi R}{\lambda}\right)^2\left(1-\left(\frac{2\pi R}{\lambda}\right)^2\right)\right], \tag{2}$$

where δ_s is surface thickness, D_s surface diffusivity, γ_s surface energy, Ω atomic volume, k Boltzmann constant, and T temperature. If any longitudinal perturbation wavelength is longer than the circumference ($\lambda > 2\pi R$), the cylinder is unstable, *i.e.*, such perturbation increases in amplitude with time. There is a wavelength $\lambda_M = \sqrt{2}(2\pi R) = 8.89R$ at which the perturbation reaches a maximum value and dominates the evolution of cylinder morphology. The segmentation of a void cylinder into periodic or nonperiodic droplets at high temperatures has been reported in alumina (Gupta, 1978) and Ca-doped sapphire (Glaeser, 2001). The segmentation of a cylinder into droplets is energetically favored because of the strong tendency towards lowering the total surface area of the chain. The large $D_s\gamma_s$ in the porous tracks is the cause of the segmentation (Glaeser, 2001).

The ability to observe the same track allows us to more precisely compare the volume change of the periodic segmentation before and after heating (Fig. 4c and d). The quasi-cylindrical track decays into a sequence of spherical droplets with average radius of ~1.6R and average interval of ~13R (R, initial track radius of 2.2 nm). The total volume of the droplets decreases to approximately 47% to the track volume before annealing. Therefore, the thermal treatment also causes the shrinkage of porous tracks, in addition to the periodic segmentation.

3.2. In situ thermal annealing

The rate for track annealing can be determined by comparing the morphology of the same tracks before and after heating in an *ex situ* thermal annealing experiment under TEM. However, this method

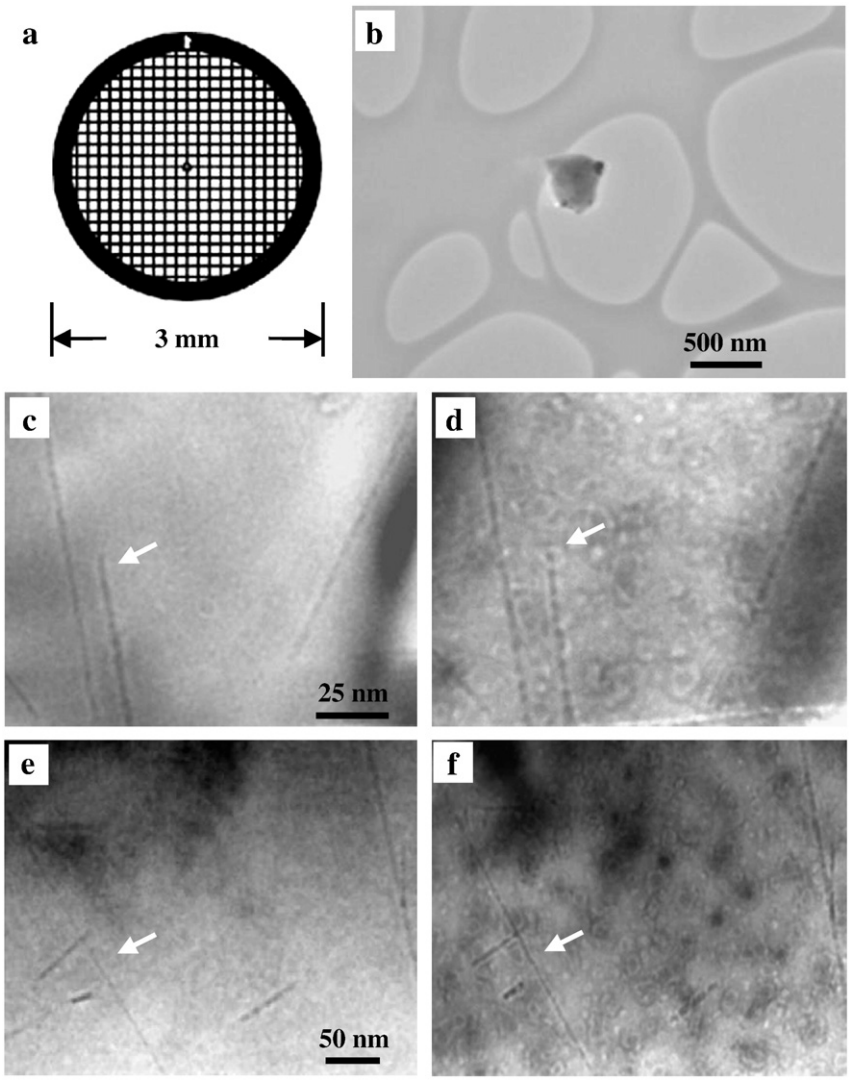

Fig. 3. The same latent fission tracks in apatite shown after *ex situ* furnace heating at 400 °C for 2 h by the register marks made on the copper grid. (a) Copper grid, (b) particle on carbon film. (c–d) The TEM images showing fission tracks in a particle before and after heating. (e–f) Fission tracks in another particle before and after heating. The TEM images are taken at slightly over focus condition. Arrows point to the tracks where some changes in tracks may be seen after heating.

cannot be used to directly observe the dynamic process, which is critical to understanding the physics of the mechanism involved in thermal annealing. *In situ* thermal-radiolytic annealing of fission tracks has been previously reported by using a TEM at temperatures up to 75 °C (Paul and Fitzgerald, 1992). However, at such low heating temperatures, it would take up to tens of millions of years (Gleadow et al., 2002) to find an observable change under the TEM. Therefore, the track fading observed in their work was actually induced by the electron beam instead of the thermal treatment (Paul, 1993a). We performed *in situ* thermal annealing of fission tracks in apatite by using a TEM specimen-heating holder at temperatures up to 1000 °C. Between the recording of TEM images, the electron beam was moved away in order to reduce the effects of electron–irradiation-induced annealing.

We first performed *in situ* thermal annealing of tracks created in zircon by 2.2 GeV Au ions (Fig. 5). After heating at 700 °C for 21 min, there was no apparent change in the morphology of the tracks in zircon (Fig. 5a and b). When the heating temperature was increased to 800 °C for additional 16 min heating, the shrinkage of tracks was evident, but not significant (Fig. 5c). Once the temperature was increased to 900 °C and stabilized for another 3 min, the tracks disappeared rapidly (Fig. 5d). This experiment confirms that an increase of the annealing temperature can significantly reduce the annealing time, which is consistent with the results of optical observations of etched tracks (Green et al., 1986; Yamada et al., 1995). This result also suggests that one may find a suitable temperature between 800 and 900 °C at which to observe the change in shape of tracks in zircon as a function of time.

A fixed annealing temperature at 830 °C was selected for *in situ* thermal annealing of amorphous tracks in zircon (Fig. 6a–d). The TEM images clearly show the dynamic process of the thermal annealing of the amorphous tracks in zircon (Li et al., 2010). The amorphous tracks gradually become narrower and eventually disappear at 90 min. These observations of the gradual fading process are consistent with the common theoretical assumption that the annealing of the amorphous tracks is a defect-elimination process by minor atomic repositioning (Carlson, 1990; Fleischer, 2004). However, no track segmentation during the annealing was observed in the amorphous tracks (Fig. 6a–d), which is significantly different from the porous tracks in apatite. As compared to those of the porous tracks, the surface energy and the diffusivity of atoms at the surface of the amorphous domains of the tracks are too low to allow the segmentation of a track into separate droplets.

In order to further investigate the differences between the thermal annealing behavior of amorphous *vs.* porous tracks, an *in situ* thermal annealing experiment of porous fission tracks in apatite was conducted by heating the sample at 700 °C (Fig. 6e–h). Dark spots from the copper

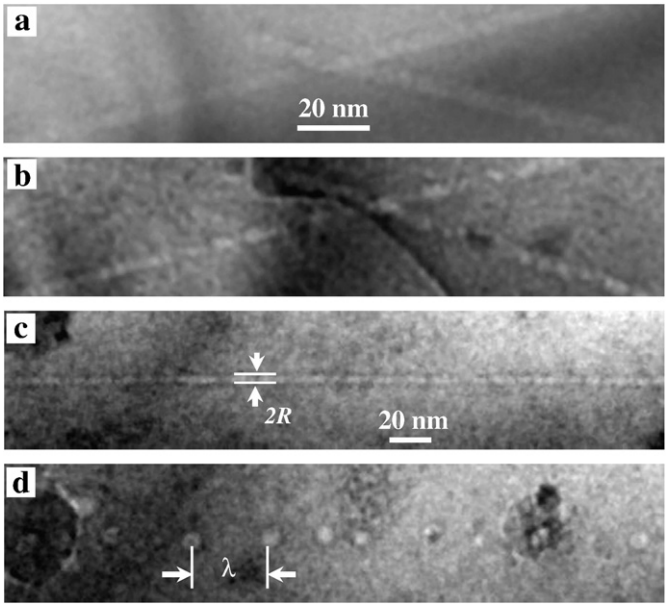

Fig. 4. The segmentation and shrinkage of fission tracks in apatite is shown after *ex situ* furnace heating at 700 °C for 2 h. (a to b) TEM images of two fission tracks in a particle before and after heating. The tracks shrink and segment into separate droplets without much periodicity. (c to d) TEM images of a fission track in another particle before and after heating showing periodic segmentation, which agrees with Rayleigh instability model. *R*, initial track radius, λ, spacing between segmented droplets.

grid deposited onto the sample surface once the temperature stabilized at 700 °C. Some fission tracks were filled with copper nano-rods due to capillary effects at elevated temperature (Borowiak-Palen et al., 2006),

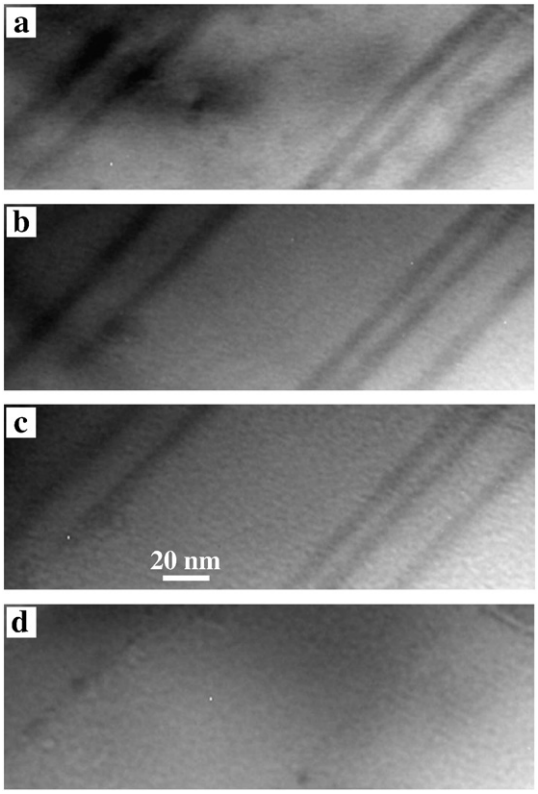

Fig. 5. *In situ* thermal annealing of 2.2 GeV Au ions induced tracks in zircon at different temperatures observed by TEM. (a) Room temperature, (b) after heating at 700 °C for 21 min, (c) additional heating at 800 °C for 16 min, and (d) further heating at 900 °C for 3 min. The change in track morphologies is insignificant and slow at or below 800 °C, while the change is obvious at 900 °C.

providing additional evidence of their porous nature. Similar copper nano-rods have been seen to form in the hollow channels of carbon nano-tubes after heating at 600 °C for 8 h (Zhang and Su, 2009). The thermal annealing behavior of the porous tracks in apatite is significantly different from that of amorphous tracks in zircon (Li et al., 2010). Initially, the track radius either shrinks or grows along the ion trajectory without much periodicity in the intervals (Fig. 6f, after 1 min). After annealing times in excess of 53 min (Fig. 6g), the fission track breaks into segments, randomly fragmented along the ion trajectory. Brownian motion of helium gas bubbles in a vanadium metal has been previously demonstrated by *in situ* TEM with a heating stage (Tyler and Averback, 1980). It is the random motion of atoms on the void surface and the large surface energy of voids that account for the random movement of voids and bubbles (Olander, 1976). The different annealing behaviors of the porous tracks in apatite as compared with the amorphous tracks in zircon are consistent with the significant differences in their internal structure.

The mean lengths of etched tracks parallel to the *c*-axis (l^c) in apatite were found to be slightly larger than those that are perpendicular to the *c*-axis (l^a) (Green et al., 1986,). Donelick et al. reported that l^c is greater than l^a in all cases (even at room temperatures), the difference increasing systematically and continuously as the degree of partial track annealing increases (Donelick, 1991). TEM observations of latent fission tracks in apatite show that the average diameter of tracks along the *c*-axis is found to be ~9 nm, obviously larger than that of tracks (~5 nm) perpendicular to the *c*-axis (Paul and Fitzgerald, 1992). The formation of larger tracks along the *c*-axis has been explained as a result of the anisotropy in the dielectric constants, 9.65 perpendicular to the *c*-axis and 7.75 parallel to the *c*-axis (Rabone et al., 2008). A moving charge has the greatest effect on the surrounding ions in the directions perpendicular to its motion. The electric field of a charge moving parallel to the *c*-axis interacts more strongly with the ions closer to the trajectory than a charge moving perpendicular to the *c*-axis, resulting in the larger tracks along this axis (Rabone et al., 2008). However, the anisotropic annealing behavior of fission tracks has been explained as a result of the anisotropic diffusivity (Gleadow et al., 2002) instead of the anisotropic dielectric constants (Rabone et al., 2008). The channels along the *c*-axis of hexagonal structure of fluroapatite favor transport of diffusing species, resulting in more rapid annealing of tracks perpendicular to the *c*-axis (Gleadow et al., 2002; Green et al., 1986). Track formation is different from track annealing, but the quench of the hot vapor zone during track formation (Chadderton, 2003) is actually an extremely rapid annealing process. This anisotropic quench during track formation likely causes larger tracks along the *c*-axis as observed by TEM (Paul and Fitzgerald, 1992). However, direct observations of the dynamic process of track annealing in different directions are extremely important for unraveling the actual mechanism involved in the crystallographic effect. We observed the preferential motion of track segments in fluorapatite at 700 °C in an *in situ* thermal annealing experiment (Fig. 7). The breakup of the track perpendicular to the *c*-axis into segments is faster and more obvious than that parallel to the *c*-axis (Li et al., 2010). The segments move and elongate along the *c*-axis. The preferential motion of the segments of a track almost perpendicular to the *c*-axis results in the formation of several parallel segments along the *c*-axis, which rotate almost 90° from the original ion trajectory (Fig. 7d). The preferential motion of fission-track segments along the *c*-axis contributes to the slower annealing and longer etched lengths of tracks along the *c*-axis.

4. Discussion

4.1. Differences between optical and TEM observations of fission tracks

The thermal annealing rate for unetched tracks in apatite has been considered not to be consistent with that of tracks after being annealed and chemical etched based on the differences between the TEM observations of unetched tracks and the optical observations of

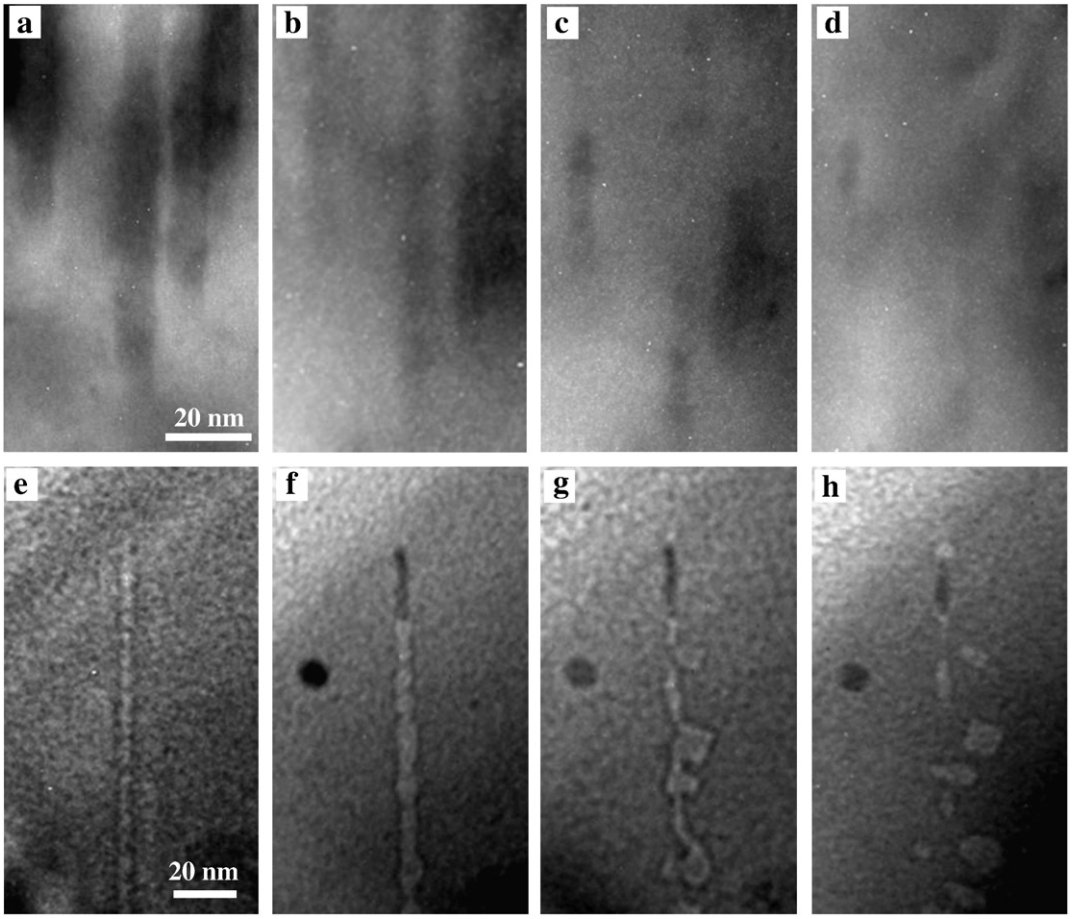

Fig. 6. *In situ* isothermal annealing of latent tracks in zircon and apatite observed by TEM. (a–d) At 830 °C, the amorphous tracks created by 2.2 GeV ions in zircon gradually disappear without track segmentation; (a) before heating, and (b) after 10, (c) 53 and (d) 90 min. (e–h) At 700 °C, a porous fission track in apatite gradually segments into shorter lengths; (e) before heating, and (f) after 1, (g) 53 and (h) 130 min. Copper "spots" from the TEM grid deposit on sample surface, and the copper nano-rods fill in the porous fission track.

etched tracks (Paul, 1993b). However, this inconsistency actually implies that TEM-observable damage remains in minerals well after etchable tracks have disappeared because of thermal treatment. This is also reflected in the range difference between etched tracks and latent tracks immediately after a fission event (Fleischer, 2004; Price et al., 1968). Before discussing the reasons for this apparent inconsistency observed in apatite, one should clarify the differences between the two methods.

First, the annealing rate of etchable tracks is determined by measuring the mean lengths of many etched tracks as observed by an

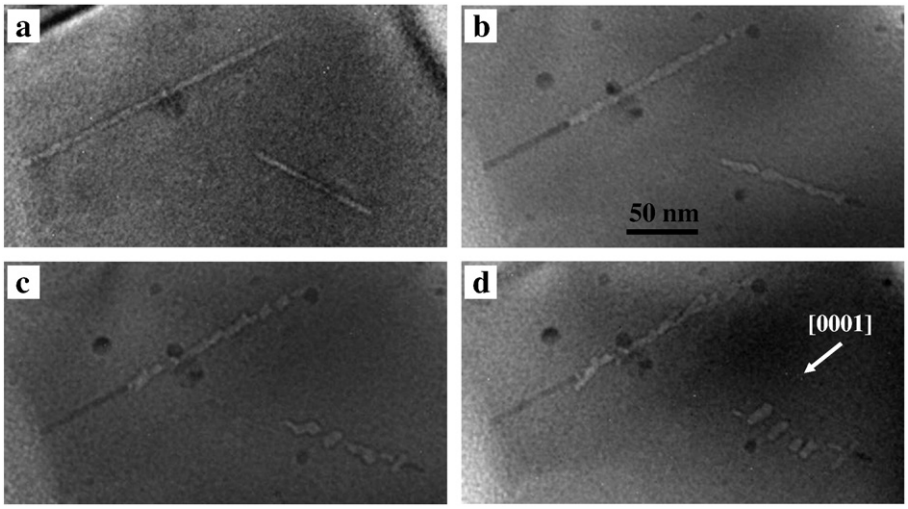

Fig. 7. *In situ* TEM images showing the preferential motion of fission track segments along [0001] (or the *c*-axis) of fluorapatite and the slower fragmentation of tracks along this axis during thermal treatment at 700 °C. (a) Before annealing, (b) after 1, (c) 17 and (d) 60 min.

optical microscope; while the measurement of latent tracks is determined by comparing the shape change of individual tracks as observed by TEM. The optical microscope allows one to observe the entire length of etched tracks. In contrast, the lengths of individual tracks that can be observed by TEM are limited by the thickness of the TEM sample and the field-of-view on the TEM viewing screen. Therefore the track lengths that can be directly observed under TEM are usually shorter than 1 μm. It is not appropriate to use the measured track lengths as determined by TEM in order to determine the annealing rate.

Second, one can observe the dynamic process of annealing of latent tracks under TEM, but it is impossible to observe them for chemically etched tracks. The morphology of a fission track is permanently changed by etching because the etching solution removes both the track core and some of the surrounding solid (Crowley et al., 1991). In addition, chemical etching can induce errors in the length measurements because the etched length of tracks is controlled, not only by the latent track length, but also by the solution composition and the etching time (Crowley et al., 1991). Furthermore, the actual change of track morphology depends on many factors, such as the annealing temperature, the track radius, its crystallographic orientation to the surrounding material, the gas content within the track, and even the uniformity of the track along the ion trajectory. Therefore, direct TEM observation allows one to determine different annealing behaviors for individual fission tracks. By observing etched tracks, one can reveal the difference in final lengths of individual tracks after the etching, but not their detailed annealing behavior.

Despite the differences discussed earlier, the time and temperature for the completion of the loss of latent tracks in zircon obtained by TEM observation are actually consistent with that observed for the chemically etched tracks. Direct TEM observation shows that the amorphous tracks in zircon almost disappear at 830 °C after 90 min, which is consistent with the completion of the fading of etchable tracks at 800 °C after 60 min (Yamada et al., 1995). The amorphous tracks in zircon do not segment, and fade in a continuous way at elevated temperatures due to the recombination of vacancies and interstitials within the track. The relatively simple annealing mechanism accounts for the good correlation between the latent and etched tracks in zircon. However, the etchable tracks are annealed both at lower temperature (800° *vs.* 830 °C) and in a shorter time (60 *vs.* 90 min) than are the latent tracks. Given the potential uncertainties in comparing these two measurements, there is the possibility that after annealing for certain temperatures and times, radiation damage in zircon is still present and visible under TEM, but no longer etchable. In contrast, there is a significant discrepancy in the completion of track disappearance between the latent and etched tracks in apatite. Based on micro-scale studies on chemically etched-tracks, it has been generally believed that etchable fission tracks in apatite completely disappear at temperatures of ~360 °C within 1 h (Crowley et al., 1991; Green et al., 1985, 1986). However, remnants of the tracks as demonstrated by TEM observations of latent track annealing, in the form of isolated segments, are still present at 700 °C even after times in excess of 130 min. During track formation, the track becomes discontinuous at each end of a track where the stopping power (energy loss per unit length, dE/dx) is lower than a threshold, resulting in the shorter lengths of etched tracks as compared with the calculated ranges (Meftah et al., 1993; Villa et al., 1999). Similarly, the discontinuities of tracks in apatite, due to the track annealing, impede the etching agent from reaching the entire track, thereby significantly reducing the effectiveness of chemical etching. It is still possible that the etchable tracks in zircon disappear at slightly lower temperatures than the latent tracks. However, this difference in annealing temperature is not as significant as that observed for apatite because tracks in zircon do not segment. Etched tracks of zircon and apatite are both widely used for fission track dating, but this difference in the annealing behavior of latent tracks between these two important minerals has not been previously noted.

4.2. Mechanisms of track annealing for amorphous and porous tracks

Due to a lack of direct experimental observation, track annealing in apatite has generally been described as an atom-by-atom recovery of damage by the recrystallization of the amorphous core, similar to the process observed in the epitaxial recrystallization of other target materials (Carlson, 1990; Fleischer, 2004). This results in the gradual reduction of the observed etched track length. Based on the enhanced understanding of the internal structure and thermal annealing of latent tracks by TEM observations, we propose different mechanisms for the thermal annealing of porous *vs.* amorphous tracks.

Both the amorphous and the porous tracks shrink in size at elevated temperatures, but the mechanisms are different. For tracks in zircon, the damage recovery within the core of the amorphous track results from the recombination of vacancies and interstitials at elevated temperature (Fig. 8a). The atom-by-atom damage recovery causes the gradual reduction of track length and gradual reduction of track radius (Fleischer, 2004). In contrast, the shrinkage of the porous tracks results from the thermal emission of vacancies from the track (Fig. 8b). The gradual decrease in size and eventual disappearance of H_2 bubbles in alumina has been observed *in situ* by heating the sample up to 225 °C (Furuno et al., 1991). The growth/shrinkage of a gas-free cavity (a void) is controlled by diffusion of vacancies and interstitials between the bulk solid and the void surface, which can be expressed as (Olander, 1976),

$$\dot{R} = \frac{dR}{dt} = \frac{\Omega}{R}\left\{D_V\left[C_V - C_V^{eq}\ exp\left(\frac{2\gamma_s\Omega}{RkT}\right)\right] - D_i C_i\right\}, \quad (3)$$

where R is void radius, C_V and C_i concentrations of vacancies and interstitials in the bulk solid, D_V and D_i vacancy and interstitial diffusivity, and C_V^{eq} equilibrium vacancy concentration. The vacancy concentration at the void surface (the second term in the bracket of Eq. (3)) has been taken as that corresponding to thermodynamic equilibrium in a solid under a negative hydrostatic stress $2\gamma_s/R$. The interstitial concentration at the void surface is effectively zero. Similar to void-shrinkage, the shrinkage of porous tracks can be neglected at low temperatures due to the low vacancy diffusivity and the low equilibrium concentration of vacancies. Whereas, at high temperatures, the porous tracks tend to evaporate rather than grow because of the rapid increase in vacancy diffusivity and the equilibrium vacancy concentration, thus making thermal emission of vacancies from the porous tracks more favorable (Olander, 1976). However, shrinkage due to thermal emission can change to pressure-enhanced growth at high temperatures when the void contains gas and the internal pressure is larger than $2\gamma_s/R$ (Olander, 1976). The growth of the porous tracks in apatite was noted at the initial stages of thermal annealing at 700 °C (Figs. 6e and f, and 7a and b), suggesting the possible existence of a gaseous phase within the track.

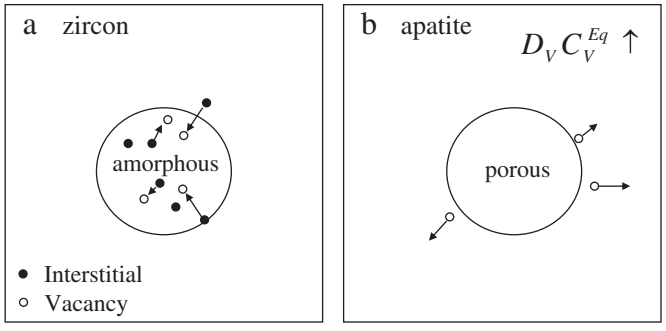

Fig. 8. Comparison of shrinkage mechanism of fission tracks in zircon to that in apatite. (a) The amorphous track in zircon shrinks by recombination of vacancies and interstitials in the core. (b) The porous track in apatite shrinks by thermo-emission of vacancies from the track to the matrix because the significant increase in the product of equilibrium of vacancy concentration and vacancy diffusivity at high temperatures.

The porous tracks in apatite may contain some of the decomposed volatile elements from the matrix during the track formation, or may be filled with gas via interactions with the solid at elevated temperatures or even with the external atmosphere; however this has not confirmed (Li et al., 2010).

The annealing process of the amorphous tracks is not as complex as that of the porous tracks (Fig. 9a). The composition of an amorphous track is not significantly different from that of the surrounding solid. The small chemical difference results in a low surface tension and the low mobility of atoms along the track surface. This structure does not favor track segmentation. Therefore, defect recombination is the main mechanism for the decrease in size of the amorphous track at elevated temperatures.

In contrast, the thermal annealing of porous tracks in apatite is a very complicated process with several underlying mechanisms (Fig. 9b). The porous structure of latent tracks is critical to providing an adequate physical description for fission track annealing in fluorapatite at elevated temperatures. The thermal emission of vacancies from the porous tracks into the matrix accounts for the decrease in track size. Further, the porous tracks become discontinuous either due to the mechanisms of Rayleigh instability, Brownian motion or preferential motion of track segments. The high surface energy of the porous tracks and their high diffusivity account for the segmentation of tracks and the movement of the track segments. In addition to the decrease in track size, the discontinuity of porous tracks significantly reduces the effectiveness of chemical etching, resulting in the shorter etched track lengths. Surface diffusion is an important mechanism by which voids (or bubbles) in the materials move randomly or preferentially along specific directions if there is potential gradient (Olander, 1976). Random motions of atoms on the surface of a void result in Brownian motion of the void. If the atoms move along in a preferred direction, the void moves preferentially along this direction (Olander, 1976). The Brownian or preferential motion results from the high surface energy and high diffusivity of atoms on the surface of voids. Similarly, the random (or preferential) motion of atoms on the porous tracks causes the random (or preferential) motion of track segments.

In order to explain the decrease in the rate of shortening over time that is observed during the isothermal annealing of etched tracks, Carlson has proposed a model of axial defect distribution, such that the defect density drops off much more rapidly with distance at small radii than for the larger radii of tracks (Carlson, 1990). According to this assumption, the defect density of a disrupted zone would gradually decrease to that of the surrounding crystal near the track boundary. However, this assumption disagrees with the sharp boundary that is observed by HRTEM (Fig. 2a and b) and in other studies (Lang et al., 2008; Vetter et al., 1998). In fact, the radius change of a fission track along the ion trajectory alone may result in the decrease of the shortening rate for isothermal annealing. An amorphous track with small radius completes defect elimination much more rapidly than that of a track with a larger radius. The fading of porous tracks is more complicated, but the faster annealing rate for the smaller radius is the same as that for amorphous tracks. According to Rayleigh instability (see Eq. (2)), the fading rate of a porous track is very sensitive to track radius, and a track with smaller radius anneals much faster. For an individual track created by a fission fragment pair, the radius is largest near its middle where the fission event occurred, and decreases toward each end of the track as the dE/dx decreases approximately linearly along the ion trajectory (SRIM, 2006). At elevated temperatures, the track begins to fade at each end, where the radii are smaller, and the fading gradually approaches that of the larger radius at the centre of the track. A calculation based on the Szenes model (Szenes, 2000) shows that the track radius is approximately proportional to,$(a-bx)^{1/2}$, a and b are constants, and x target depth along the ion trajectory. The square root relation means that, along the ion trajectory, the track's radius deceases slowly in the middle of a track, and decreases rapidly near each end of the track (as illustrated in Fig. 9). Therefore, the convex shape of the track profile can result in a decrease in the shortening rate, as has been observed by isothermal annealing of etchable tracks. The experimentally obtained profile of a latent track created by a fission fragment is not available, but this description would be more convincing if the square root relation could be confirmed. More atomic-scale studies are necessary in order to investigate the defect distribution and subsequent defect elimination processes.

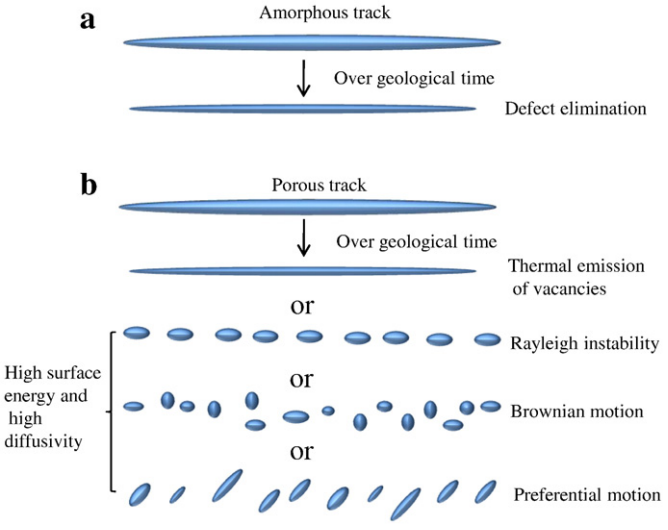

Fig. 9. Comparison of (a) track annealing mechanism of amorphous core to (b) that of porous core. The etchability of porous tracks is controlled by the gradual shrinkage and the discontinuity of fission tracks, which is either caused by Rayleigh instability, by Brownian motion or by preferential motion of track segments due to the high surface energy and high diffusivity of atoms on the inside surface of porous tracks.

5. Conclusion

We have compared the thermal annealing behavior of latent tracks in apatite and zircon by TEM. Remnants of latent fission tracks in apatite heated at 700 °C for 130 min can be observed by TEM, which is different from the observation of etchable fission tracks in apatite that are completely removed by annealing at 360 °C for 1 h (Green et al., 1986). In contrast, the complete removal of the amorphous tracks in zircon heated at 830 °C for 90 min, as observed by TEM, is similar to that of ecthable tracks, which disappear at 800 °C after 60 min (Yamada et al., 1995). Due to the high surface energy and high diffusivity of atoms in the porous tracks of apatite, these tracks segment on annealing, preventing etchant solutions from entering into the porous tracks and significantly reduce the etched track length.

In situ thermal annealing experiments of the latent tracks demonstrate that the annealing mechanisms proposed for amorphous tracks in zircon are entirely different from those of the porous tracks in apatite. Both types of tracks in apatite and in zircon decrease in size at elevated temperatures. However, the shrinkage of the track in apatite results from thermo-emission of vacancies from the porous channel, as compared with the recombination of vacancies and interstitials with an amorphous track in zircon. The high surface energy and high diffusivity of atoms on the track surface results in Rayleigh instability of the porous track, as well as Brownian or preferential motion of track segments. The random motion of atoms on the surface of porous tracks accounts for the Brownian motion of track segments. The preferential motion of atoms along the c-axis of fluorapatite causes the more rapid annealing of fission tracks perpendicular to the c-axis. The distinctive thermal annealing behavior of apatite is consistent with the porous nature of the tracks.

Acknowledgements

This paper was improved substantially by reviews and suggestions from Andrew Gleadow of School of Earth Sciences, University of Melbourne. We also thank an anonymous reviewer for the valuable comments. The funding for this study was provided by the Office of Basic Energy Sciences of the USDOE (DE-FG02-97ER45656). Maik Lang acknowledges the support from the German Research Foundation DFG.

References

Borowiak-Palen, E., Mendoza, E., Bachmatiuk, A., Rummeli, M.H., Gemming, T., Nogues, J., Skumryev, V., Kalenczuk, R.J., Pichler, T., Silva, S.R.P., 2006. Iron filled single-wall carbon nanotubes — a novel ferromagnetic medium. Chem. Phys. Lett. 421, 129–133.

Carlson, W.D., 1990. Mechanisms and kinetics of apatite fission-track annealing. Am. Mineralog. 75, 1120–1139.

Chadderton, L.T., 2003. Nuclear tracks in solids: registration physics and the compound spike. Radiat. Meas. 36, 13–34.

Crowley, K.D., 1993. Mechanisms and kinetics of apatite fission-track annealing — discussion. Am. Mineralog. 78, 210–212.

Crowley, K.D., Cameron, M., Schaefer, R.L., 1991. Experimental studies of annealing of etched fission tracks in fluorapatite. Geochim. Cosmochim. Acta 55, 1449–1465.

Donelick, R.A., 1991. Crystallographic orientation dependence of mean etchable fission track length in apatite: an empirical model and experimental observations. Am. Mineralog. 76, 83–91.

Fleischer, R.L., 2004. Fission tracks in solids—production mechanisms and natural origins. J. Mater. Sci. 39, 3901–3911.

Fleischer, R.L., Price, P.B., Walk, R.M., 1975. Nuclear Tracks in Solids. Unversity of California Press, Berkeley, p. 31.

Furuno, S., Hojou, K., Otsu, H., Izui, K., Kamigaki, N., Kino, T., 1991. In-situ observation of the dynamic behavior of bubbles in aluminum during 10 keV H_2^+ ion irradiation and successive annealing. J. Nucl. Mater. 179–181, 1011–1014.

Glaeser, A.M., 2001. Model studies of Rayleigh instabilities via microdesigned interfaces. Interface Sci. 9, 65–82.

Gleadow, A.J.W., Duddy, I.R., Green, P.F., Lovering, J.F., 1986. Confined fission track lengths in apatite: a diagnostic tool for thermal history analysis. Contrib. Mineralog. Petrol. 94, 405–415.

Gleadow, A.J.W., Belton, D.X., Kohn, B.P., Brown, R.W., 2002. Fission track dating of phosphate minerals and the thermochronology of apatite. Rev. Mineral. Geochem. 48, 579–630.

Green, P.F., Duddy, I.R., Gleadow, A.J.W., Tingate, P.R., Laslett, G.M., 1985. Fission-track annealing in apatite: track length measurements and the form of Arrhenius plot. Nucl. Tracks 10, 323–328.

Green, P.F., Duddy, I.R., Gleadow, A.J.W., Tingate, P.R., Laslett, G.M., 1986. Thermal annealing of fission tracks in apatite 1. A qualitative description. Chem. Geol. 59, 237–253.

Green, P.F., Laslett, G.M., Duddy, I.R., 1993. Mechanisms and kinetics of apatite fission-track annealing — discussion. Am. Mineralog. 78, 441–445.

Gupta, T.K., 1978. Instability of cylindrical voids in alumina. J. Am. Ceram. Soc. 61, 191–195.

Jaskierowicz, G., Dunlop, A., Jonckheere, R., 2004. Track formation in fluorapatite irradiated with energetic cluster ions. Nucl. Instrum. Meth. Phys. Res. B 222, 213–227.

Jonckheere, R.C., Chadderton, L.T., 2002. Back to Basic? On track: The Newsletter of the International Fission-Track Community, 12, 19 p.

Lang, M., Lian, J., Zhang, F.X., Hendriks, B.W.H., Trautmann, C., Neumann, R., Ewing, R.C., 2008. Fission tracks simulated by swift heavy ions at crustal pressures and temperatures. Earth Planet. Sci. Lett. 274, 355–358.

Laslett, G.M., Green, P.F., Duddy, I.R., Gleadow, A.J.W., 1987. Thermal annealing of fission track in apatite, 2. A quantitative analysis. Chem. Geol. 65, 1–13.

Li, W., Wang, L., Sun, K., Lang, M., Trautmann, C., Ewing, R.C., 2010. Porous fission fragment tracks in fluorapatite. Phys. Rev. B 82, 144109.

Meftah, A., Brisard, F., Costantini, J.M., Hage-Ali, M., Stoquert, J.P., Studer, F., Toulemonde, M., 1993. Swift heavy ions in magnetic insulators: a damage cross section velocity effect. Phys. Rev. B 48, 920.

Miro, S., Grebille, D., Chateigner, D., Pelloquin, D., Stoquert, J.P., Grob, J.J., Costantini, J.M., Studer, F., 2005. X-ray diffraction study of damage induced by swift heavy ion irradiation in fluorapatite. Nucl. Instrum. Meth. Phys. Res. B 227, 306–318.

Nichols, F.A., Mullins, W.W., 1965. Surface-(interface-) and volume-diffusion contributions to morphological changes driven by capillarity. Trans. Metall. Soc. AIME. 233, 1840.

Olander, D.R., 1976, Fundamental Aspects of Nuclear Reactor Fuel Elements: Springfield, Virginia, National Technical Information Service, U.S. Department of Commerce, 236–239, 490–491 p.

Paul, T.A., 1993a. Atomic Scale Investigation of Latent Fission Tracks In Fluorapatite: Physical Characteristics and Annealing Behavior. Arizona Unate University, U.S.A.

Paul, T.A., 1993b. Transmission electron microscopy investigation of unetched fission tracks in fluorapatite-physical process of annealing. Nucl. Tracks Radiat. Meas. 21, 507–511.

Paul, T.A., Fitzgerald, P.G., 1992. Transmission electron microscopic investigation of fission tracks in fluorapatite. Am. Mineralog. 77, 336–344.

Price, P.B., Walker, R.M., 1962a. Electron microscope observation of a radiation-nucleated phase transformation in mica. J. Appl. Phys. 33, 2625–2628.

Price, P.B., Walker, R.M., 1962b. Observations of charged-particle tracks in solids. J. Appl. Phys. 33, 3400–3406.

Price, P.B., Fleischer, R.L., Moak, C.D., 1968. Identification of very heavy cosmic-ray tracks in meteorites. J. Appl. Phys. 167, 277.

Rabone, J.A.L., Carter, A., Hurford, A.J., de Leeuw, N.H., 2008. Modelling the formation of fission tracks in apatite minerals using molecular dynamics simulations. Phys. Chem. Miner. 35, 583–596.

Saleh, S.A., Eyal, Y., 2005. Porous track cores along wakes of swift Pb ions in LiF. Nucl. Instrum. Meth. Phys. Res. B 230, 246–250.

Shuster, D.L., Flowers, R.M., Farley, K.A., 2006. The influence of natural radiation damage on helium diffusion kinetics in apatite. Earth Planet. Sci. Lett. 249, 148–161.

SRIM, 2006. http://www.srim.org/SRIM/SRIM2006.htm.

Szenes, G., 2000. Analysis of tracks induced by cluster ions in CaF_2. Phys. Rev. B 14267.

Tagami, T., O'Sullivan, B., 2005. Fundamentals of fission track thermochronology. Rev. Mineral. Geochem. 58, 19–47.

Tyler, S.K., Averback, R.S., 1980. Direct evidence for the Brownian motion of helium bubbles. J. Nucl. Mater. 92, 201.

Vetter, J., Scholz, R., Dobrev, D., Nistor, L., 1998. HREM investigation of latent tracks in GeS and mica induced by high energy ions. Nucl. Instrum. Meth. Phys. Res. B 141, 747–752.

Villa, F., Grivet, M., Rebetez, M., Dubois, C., Chambaudet, A., Chevarier, A., Martin, P., Brossard, F., Blondiaux, G., Sauvage, T., Toulemonde, M., 1999. Damage morphology of Kr ion tracks in apatite: dependence on dE/dx. Radiat. Meas. 31, 65–70.

William, D.B., Carter, C.B., 1996. Transmission Electron Microscopy. Plenum Press, New York and London, 82–451 pp.

Yamada, R., Tagami, T., Nishimura, S., Ito, H., 1995. Annealing kinetics of fission tracks in zircon: an experimental study. Chem. Geol. 122, 249–258.

Zhang, Z., Su, D., 2009. Behaviour of TEM metal grids during *in-situ* heating experiments. Ultramicroscopy 109, 766–774.